Geophysical Journal International

Geophys. J. Int. (2013) **192,** 1132–1143 doi: 10.1093/gji/ggs061

Analytic approximation to the scattering of antiplane shear waves by free surfaces of arbitrary shape via superposition of incident, reflected and diffracted rays

Juan Jaramillo, Juan Gomez, Mario Saenz and Juan Vergara

Departamento de Ingeniería Civil, Universidad EAFIT, Medellín, Colombia. E-mail: jgomezc1@eafit.edu.co

Accepted 2012 November 6. Received 2012 October 4; in original form 2011 July 28

SUMMARY

The scattering induced by surface topographies of arbitrary shapes, submitted to horizontally polarized shear waves (*SH*) is studied analytically. In particular, we propose an analysis technique based on a representation of the scattered field like the superposition of incident, reflected and diffracted rays. The diffraction contribution is the result of the interaction of the incident and reflected waves, with the geometric singularities present in the surface topography. This splitting of the solution into different terms, makes the difference between our method and alternative numerical/analytical approaches, where the complete field is described by a single term. The contribution from the incident and reflected fields is considered using standard techniques, while the diffracted field is obtained using the idea of a ray as was introduced by the geometrical theory of diffraction. Our final solution however, is an approximation in the sense that, surface-diffracted rays are neglected while we retain the contribution from corner-diffracted rays and its further diffraction. These surface rays are only present when the problem has smooth boundaries combined with shadow zones, which is far from being the typical scenario in far-field earthquake engineering. The proposed technique was tested in the study of a combined hill-canyon topography and the results were compared with those of a boundary element algorithm. After considering only secondary sources of diffraction, a difference of 0.09 per cent (with respect to the incident field amplitude) was observed. The proposed analysis technique can be used in the interpretation of numerical and experimental results and in the preliminary prediction of the response in complex topographies.

Key words: Numerical solutions; Numerical approximations and analysis; Site effects.

1 INTRODUCTION

The scattering of elastic waves by irregularities of arbitrary shape is important in different engineering fields, for example, oil and natural gas industry, rock mechanics and earthquake engineering. The modifications experienced by an incident wave can be generated by two mechanisms: a geometric effect, induced by the interaction of the field with topographic discontinuities along the propagation path, and a mechanical effect, resulting from impedance contrasts in the propagation medium. This work focuses in the geometric effect. Although currently available numerical methods are capable of treating highly complex and realistic scenarios, analytic solutions are important from a conceptual and a practical point of view. Analytic solutions combined with experimental and/or numerical results, represent a powerful analysis tool to understand and elucidate the physics behind complex wave propagation problems. Here we study the scattering of horizontally polarized shear (*SH*) waves in half-spaces, with surface topographies of arbitrary shape, using an analytic approach. In the context of earthquake engineering, most of the available closed-form solutions have been restrained to idealized scenarios, with only a few contributions dealing with general arbitrary cases but in terms of complex mathematical formalisms. The main goal of this work is to describe a simple, physically based analysis methodology that provides the analyst with the ability to capture the most relevant features of the response of a complex surface topography in terms of simple input parameters.

When dealing with the scattering by irregularities of arbitrary shape, the main complexity lies in the determination of the diffracted field. As discussed by Keller (1962) , simple methods based on geometrical optics, fail to account for certain phenomena called diffraction. The diffracted field appears after incident fronts hit edges, corners or vertices of boundary surfaces. At the same time, if the involved scattering boundaries are at least C^2-continuous and also fully illuminated by the incident rays, the solution can be obtained based solely on geometrical methods. On the contrary, if there are shadow zones or corner singularities, the geometric solution by itself is discontinuous and it must be completed with the diffracted field. It turns out that the diffraction contribution to the

total displacement field, can be defined as that part of the solution that cannot be predicted by the classical geometric theory of rays. It is evident that a key aspect in the search for a general method to conduct analytic studies in scatterers with geometries of arbitrary shape is the ability to describe the diffracted field.

The physical aspects of diffraction have been studied in great detail in the context of scattering problems of electromagnetic waves. A landmark analytic contribution is identified in the work by Sommerfeld (1896) who derived the solution for the diffraction induced by a semi-infinite crack. The contribution by Sommerfeld (1896) opened the door to a number of studies dealing with the more general case of an infinite wedge, where the crack problem is a particular solution. The scattering by an infinite wedge under incident scalar and vector wavefields, involves precisely the case of wave fronts hitting edges and other singularities along boundary surfaces and it may be considered a fundamental or canonical source of diffraction. MacDonald (1902) obtained a series expansion for the total field in the wedge in terms of Bessel functions. Hudson (1963) studied the wedge under a line source of harmonic *SH* waves for combined Dirichlet and Neumann boundary conditions and expressed his solution in the form of an infinite integral. Forristal & Ingram (1971) studied elastic wedges of arbitrary angles under dynamic surface tractions; they also expressed their solution in terms of a singular integral. Abo-Zena & King (1973) solved the problem of a wedge under a line source applied along its free surface. In that solution the response was separated in terms of the incident, reflected and diffracted fields, but the diffracted term was given as a singular integral. Hong & Helmberger (1977) studied the case of a dipping structure (i.e. a layer in the form of a wedge in a half-space), with a line source embedded in the medium; the solution was expressed in terms of an infinite series. Hong & Helmberger (1978) formulated the so-called glorified optics to study waves propagating in non-planar structures. Klem-Musatov & Aizenberg (1984) also studied the infinite wedge and presented a separated solution in terms of incident, reflected and edge effects. Sanchez-Sesma (1985) reformulated the solution by MacDonald (1902), and solved the problem of *SH* waves scattered by infinite wedges, including diffraction effects. The solution was still given in terms of a single series, complicating its application to arbitrary shapes. The same approach was later used by Sanchez-Sesma & Velasquez (1987) to address the dipping layer problem and by Sanchez-Sesma *et al.* (1988) and Sanchez-Sesma (1990) to solve triangular alluvial valleys and infinite wedges in particular cases where diffraction was absent.

Although the above set of solutions consider the diffraction effect, they are valid for particular configurations. In contrast, Keller (1962) concentrated solely on the diffraction problem. He studied the interaction of incident waves with straight edges, curved edges, corners and surfaces. The relevance of that work lies in the fact that different sources of diffraction were identified and treated in relatively simple mathematical terms introducing the conceptual tool of diffracted rays.This allows the determination of the amplitude and phase at a point contributed by a diffracted ray, in terms of a diffraction coefficient, pretty much in the same way in which the contribution from a reflected or refracted ray is obtained using a reflection/refraction coefficient applied to the incident front. This theory of diffracted rays is known as the geometrical theory of diffraction (GTD) and constitutes the basis of our method.

Excluding numerical approaches, only a few analytic solutions have been proposed for general geometrical perturbations under the incidence of mechanical waves, even for the simple *SH* case. The majority of the available solutions are valid only in particular configurations or so strongly tied to complex mathematical formalisms, that its application to truly arbitrary geometries is a difficult task. For instance, the two extreme problems of scattering of *SH* waves by a canyon and a valley of semi-circular shape were solved by Trifunac (1971, 1973),in terms of expansions of Hankel functions. Todorovska & Lee (1990, 1991a,b) studied semi-spherical valleys at low frequencies, under *SH*, *SV* and Rayleigh waves. Sanchez-Sesma & Iturraran-Viveros (2001) addressed the problem of a finite crack in a half-space, under *SH* waves over a wide range of frequencies using as a fundamental block the Sommerfeld solution from electromagnetics. Lee & Luo (2006) studied *SH* waves incident against a semi-circular cylindrical hill using a series solution. Tsaur (2010) solved the problem of a vertical crack in the free surface of a half-space using separation of variables in elliptical coordinates, while Tsaur *et al.* (2010) addressed a symmetrical V-shaped canyon under incident *SH* waves. More recently, Tsaur (2011) studied the scattering and focusing of *SH* waves by a lower semi-elliptic convex topography while Diankui & Feng (1991) concentrated on cylindrical canyons of apparently arbitrary shapes over anisotropic half-spaces. In this last contribution the actual reflection problem is converted into a classical half-space reflection problem using conformal mapping. The required mathematical formalism is however cumbersome to apply in arbitrary shapes. Fu (2005) used an integral representation of the scattered field generated by an arbitrary shape under incident *SH* waves and approximated the kernels of the integral equation.

In what follows we discuss the basic theoretical aspects needed to construct the scattered field induced by an incident plane *SH* wave impinging against a free surface of arbitrary shape. The method is based on the superposition of incident, reflected and diffracted rays and therefore we focus on the description of the procedure to obtain the contribution from the diffracted field. This single term is obtained after adapting a solution from Kouyoumjian & Pathak (1974) for a generalized wedge, involving a corner singularity enclosed by curved boundaries and corresponding to an improved version of the geometric method proposed by Keller (1962). The superposition technique results in a conceptual recipe to construct the scattered field. This recipe is further detailed within the context of a general scenario and then, specifically applied to a topography consisting of a canyon–hill combination. The accuracy of the built solution is tested against numerical results obtained with a direct boundary element algorithm.

2 MATHEMATICAL MODEL AND OUTLINE OF THE METHOD

Consider the scatterer of Fig. 1 consisting of an isotropic linearly elastic homogeneous half-space with a geometric perturbation of arbitrary shape along its free surface, where β = wave propagation velocity, ρ = mass density and ν = Poisson's ratio. The mathematical domain is defined by the volume V and its enclosing surface $S_F \cup S \cup S_\infty$, where S_∞ is at infinity, and with radiation boundary conditions imposed along this surface. In this scenario the scatterer corresponds to the surface S and the total resulting wave motion depends on the incident field and on the geometry of the free surface. The system is then submitted to a plane, horizontally polarized shear wave (antiplane problem), propagating with direction $\hat{n}$. The resulting antiplane motion is of the general form $w = \hat{W} e^{-i(\vec{k}\cdot\vec{x}-\omega t)}$, where $\hat{w} = \hat{W} e^{-i\vec{k}\cdot\vec{x}}$ = displacement spectral amplitude, $i = \sqrt{-1}$, $\vec{k} \equiv \hat{n}\omega/\beta$ = wave vector, ω = circular frequency, $\vec{x}$ = position vector of an observation point and t = time. In what follows we write w instead of $\hat{w}$. The scattering problem consists in the determination of the total motions after the

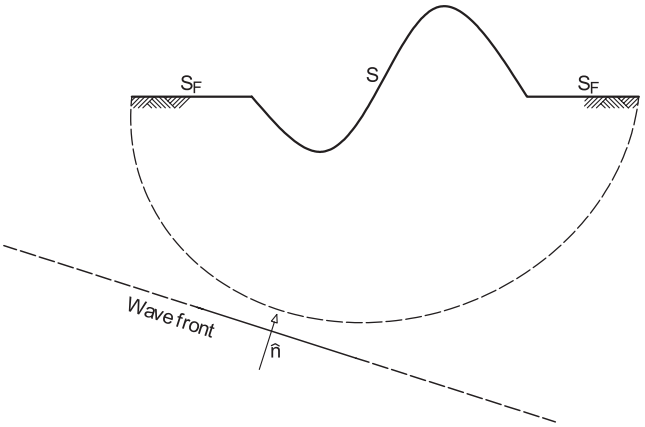

Figure 1. Mathematical domain corresponding to the half-space, the scatterer surface and the incident plane wave.

incident plane wave interacts with the free surface $S_F \cup S$. Because of the free boundary condition existing along the surface $S_F \cup S$, all the incident energy is reflected back into the half-space. If the contributions from the incident and reflected motions at an arbitrary point $\vec{x} =$ are properly added (i.e. simultaneously accounting for amplitude and phase), it turns out that the resulting displacements are discontinuous. Continuity however can be restored after the addition of an extra term corresponding to the diffraction effects.

The idea behind our solution method is to achieve the continuity in the displacements by completing the ray theory solution with the consideration of the diffracted field associated with the scattering surface S. The diffracted field is obtained after representing the complex scatterer surface by a series of simple surfaces or superposition of wedges. Each wedge contributes in the form of a source of primary diffraction. Each diffracted ray can be further reflected or diffracted as it interacts with the adjacent wedges. With the diffracted contribution at hand, the complex and general scattering problem is simply reduced to a superposition problem, where the displacement at a given point is constructed after considering the contribution of the incident plane front w^0, the reflected plane front w^R and the diffracted field w^D like

$$w = w^0 + w^R + w^D. \tag{1}$$

In our construction method the contribution w^D to the total field, is adapted from the solution developed by Kouyoumjian & Pathak (1974) and corresponding to the diffraction of an electromagnetic wave obliquely incident on an edge, in an otherwise smooth curved surface adapted from the GTD proposed by Keller (1962), that is, a generalized wedge. As pointed out by Keller (1962), whenever there are curved surfaces and shadow zones, there are also surface-diffracted rays. These rays are however neglected by the Kouyoumjian & Pathak (1974) solution leaving only the diffraction corresponding to the corner effect. That assumption yields accurate results if the field point is sufficiently far removed from the surface or if the surface itself is fully illuminated. When the surface is fully illuminated, which is the typical case in earthquake engineering, the surface-diffracted rays vanish and an approximation in terms of polygonal shapes simplifies the computation of the reflected field which is of little interest in this contribution.

Within the above simplifying assumptions the total field is completed after adding the contributions from the incident and reflected fields. This solution to the generalized wedge problem is the basis of this work. The methodology can be summarized as follows. The free surface of the half-space, containing the topographic perturbation of arbitrary shape is approximated by a superposition of finite wedges. The approximation involved in the representation of the general wedge, made up of curved boundaries, by a simple one composed of straight edges, is important only when there are shadow zones in the incident field. In such a case there are surface-diffracted rays being neglected in the current approach. That particular scenario is however unlikely to occur in far-field earthquake engineering, where the incidence can be assumed to be vertical thereby producing a fully illuminated domain. Each resulting finite wedge contributes with a reflected field plus three sources of primary diffraction: one generated by the main wedge and two additional sources, corresponding to the points where the infinite wedge is rendered finite at corner singularities. Besides from properly accounting for the primary diffracted field, the main challenge involved in the process for constructing the solution is the fact that the primary diffracted motions are further diffracted as they encounter other geometric singularities. We have selected the term secondary or higher order diffraction to refer to this additional contribution. The secondary and higher order diffraction effects can be represented by an infinite number of terms of continuously decreasing amplitude. In the actual application of the method a threshold value is selected and the higher order diffraction is stopped, once the desired accuracy is achieved, resulting in a rational approximation to the final solution. In contrast to available analytical solutions and to robust numerical methods, where as a result of the analysis the total response is obtained in a single term, in our solution method the response function is constructed by adding separate terms, each one with a different physical meaning. In this sense, and after having accounted for the contribution of the incident and reflected rays, the solution is completed after reiterated use of a fundamental case deriving in a conceptual recipe to find the response of the system. In this way the recipe, has the final potential to capture the response of a problem with a complex geometry in relatively simple terms.

3 FUNDAMENTAL SOLUTION: THE DIFFRACTED RAYS

The process of superposition of the fields is now explained with reference to the general problem described in Fig. 2, where the relevant illuminated and shadow domains and its corresponding boundaries are detailed. Consider a plane *SH* wave incident against the free surface of the wedge at an angle ϕ'. This angle is formed between the propagation direction and the surface of the wedge. The incident wave is described by the plane front, which in terms of rays is equivalent to the group of infinite incident rays perpendicular to the front. It is of interest to identify the incidence and reflection boundaries corresponding to planes of discontinuity in the solution, contributed by the incident and reflected fields. The diffracted field generated by the corner singularity corresponds to a cylindrical wave that penetrates into the shadow zone and restores continuity along the reflection and incidence boundaries.

The contribution from the incident and reflected fields considered must be completed by the diffracted part of the solution w^D. This addition renders continuous the motion calculated from the incident and reflected rays and penetrates into the shadow zone, that is, the term w^D provides the proper transition between the illuminated and the shadow zones. In the proposed methodology, the contribution of the diffracted field is taken directly from the approximate solution proposed by Kouyoumjian & Pathak (1974) and corresponding to a generalized infinite wedge submitted to an incident plane or cylindrical wave. The case of a cylindrical diffraction front corresponds to a previously diffracted field. The generalized solution for

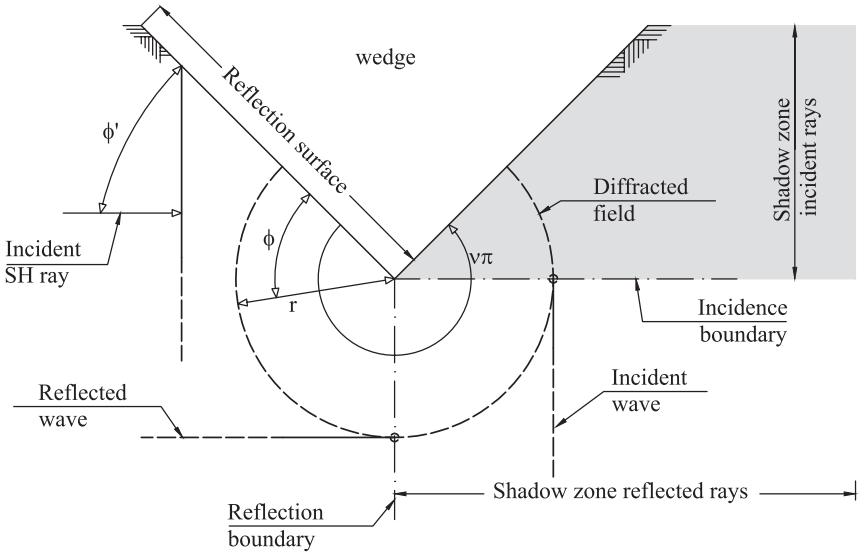

Figure 2. Plane SH wave incident against an infinite wedge. The region of existence of the incident rays corresponds to the illuminated zone. As the incident front is reflected by the free surface a zone illuminated by the reflected rays develops. The superposition of these two fields is discontinuous, however continuity is restored by the cylindrical diffracted field that penetrates into the shadow zone.

the diffracted field is given in (2) for a field point with coordinates (ϕ, r) as follows:

$$w^{\mathrm{D}}(\phi, r) = A\frac{-\mathrm{e}^{(-\hat{\imath}(kr+\pi/4))}}{2\nu\sqrt{2\pi}\sqrt{kr}}\left[\cot\left(\frac{\pi+(\phi-\phi')}{2\nu}\right)F\left(k\mathrm{La}^{+}\left(\phi-\phi'\right)\right)\right.$$
$$+\cot\left(\frac{\pi-(\phi-\phi')}{2\nu}\right)F\left(k\mathrm{La}^{-}\left(\phi-\phi'\right)\right)$$
$$+\cot\left(\frac{\pi+(\phi+\phi')}{2\nu}\right)F\left(k\mathrm{La}^{+}\left(\phi+\phi'\right)\right)$$
$$\left.+\cot\left(\frac{\pi-(\phi+\phi')}{2\nu}\right)F\left(k\mathrm{La}^{-}\left(\phi+\phi'\right)\right)\right], \tag{2}$$

where r = radial coordinate to the field point measured from the vertex of the wedge, ϕ = angular coordinate measured with respect to the reflection boundary, ϕ' = incidence angle measured with respect to the reflection boundary, $\nu\pi$ = wedge angle, r' = radius of the incident cylindrical wave (for the diffraction of a cylindrical front), k = wavenumber and β = velocity of wave propagation. The remaining terms appearing in (2) are defined as

$$F(X) = 2\hat{\imath}\sqrt{X}\mathrm{e}^{\hat{\imath}X}\int_{\sqrt{X}}^{\infty}\mathrm{e}^{-\hat{\imath}\tau^2}\mathrm{d}\tau,$$

$$L = r \qquad \text{for incident plane waves,}$$

$$L = \frac{rr'}{r+r'} \qquad \text{for incident cylindrical waves,}$$

$$a^{\pm}(\theta) = 2\cos^2\left(\frac{2\nu\pi N^{\pm}-\theta}{2}\right),$$

$$N^{+} = \begin{cases} 0 & \text{if} \quad \theta \le \nu\pi - \pi \\ 1 & \text{if} \quad \theta > \nu\pi - \pi \end{cases},$$

$$N^{-} = \begin{cases} -1 & \text{if} \quad \theta < \pi - \nu\pi \\ 0 & \text{if} \quad \pi - \nu\pi \le \theta \le \pi + \nu\pi \\ 1 & \text{if} \quad \theta > \pi + \nu\pi. \end{cases}$$

From the solution described in (2) it is clear that the diffraction yields a cylindrical front and that for values of ϕ corresponding to points far removed from the incidence and reflection boundaries, the amplitude decays with $1/\sqrt{kr}$. On the other hand, right at the incidence/reflection boundary the diffracted field is discontinuous. This is a required condition that must be satisfied by the term w^{D} to match the corresponding discontinuity appearing in the superposition of the incident and reflected contributions.

4 EXTREME CASES

The following observations, corresponding to extreme cases of the solution given by Kouyoumjian & Pathak (1974), and useful in the application and conceptual understanding of the described technique (Kouyoumjian & Pathak 1974) are identified:

(i) Far-field behaviour: Fig. 3 describes the case when $r \to \infty$ and $1 < \nu < 2$. In this case the diffracted field, just at the incidence and reflection boundaries, approaches $\pm 0.5\mathrm{e}^{-\hat{\imath}kr}$. This corresponds to half the amplitude of the incident wave and where the + and − signs represent the phase in the shadow and illuminated zones, respectively. This result clearly restores the continuity of the displacement contributed by the incident and reflected fields.

(ii) Semi-infinite crack: Fig. 4 corresponds to the case where $r \to 0$ and $\nu = 2$. In this case the diffracted field takes a value of $+1$ in the shadow zone of the incident wave, a value of -1 in the illuminated zone of the reflected wave and a value of 0 in the zone located in-between the reflection and incidence boundaries. As the wedge angular parameter ν decreases and the crack approaches a wedge, the above results are slightly modified taking values greater than $+1$ in the shadow zone of the incident wave and values greater than -1 and smaller than 0 in the illuminated zone of the reflected wave. In the intermediate zone, the field takes values that maintain continuity of the total resulting solution.

(iii) Fig. 5 corresponds to the case $r \to 0$ and $\pi > \phi' > \pi(\nu - 1)$, while $1 < \nu < 2$ (i.e. complete illumination by the incident ray): two reflection boundaries joined together by a diffracted field (with an amplitude smaller than $+1.0$ in the zone between the boundaries and greater than -1.0 and smaller than 0.0 between the boundaries and the wedge) are generated.

(iv) Half-space: If $\nu = 1.0$ then the diffracted field $w^{\mathrm{D}} \to 0.0$ and the contribution from the incident and reflected rays is continuous.

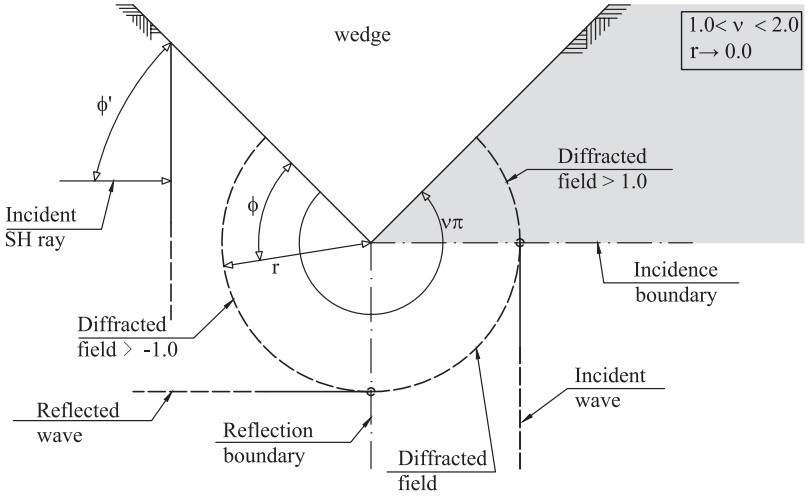

Figure 3. Extreme case corresponding to the far-field behaviour.

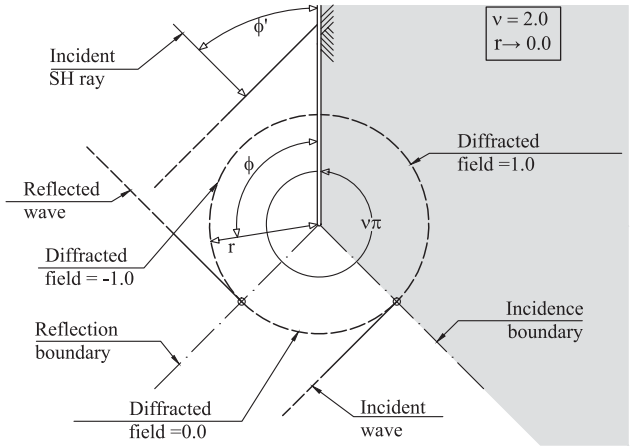

Figure 4. Particular case when the generalized wedge becomes an infinite crack.

(v) Fig. 6 corresponds to the case when $r \to 0.0$, $\nu \to 1.0$ and $\phi' \to 0.0$ (i.e. incident rays parallel to the free boundary of the wedge): a small shadow zone develops where the diffracted field approaches a value of $+2.0$ in the shadow zone, a value of $+1.0$ between the reflection and incidence boundaries and 0.0 in the zone illuminated by the reflected field. In the extreme case in which $\phi' = 0$ half the amplitude is assigned to the incident ray and half the amplitude to the reflected ray, to yield a diffracted field approaching $+1.0$ in the shadow zone and 0.0 in the remaining part of the domain. For intermediate values of kr the diffracted field takes values in between the ones defined for $r \to 0.0$ and $r \to \infty$. Depending on the location of the field point with respect to the wedge, the wedge geometry and the direction of the incident front, the amplitudes of the diffracted rays oscillate between 0.0 and 2.0. The maximum value of 2.0 is attained only at the wedge apex, for wedges with an angle close to 180° and when the incident ray is parallel to the free surface. As we move away from the apex the diffracted field modifies the shape of the pulse since there is a geometric attenuation effect inversely proportional to $\sqrt{kr}$. This means that as we move further away from the apex the high-frequency content is damped out and the pulse appears smoother. In a practical application this behaviour may be useful when trying to identify the specific part of the motion due to diffraction.

(vi) Fig. 7 corresponds to the case when $\nu < 1.0$ (i.e. propagation inside an infinite wedge): the diffracted field reaches values which are close to the amplitude of the incident wave. On the other hand,

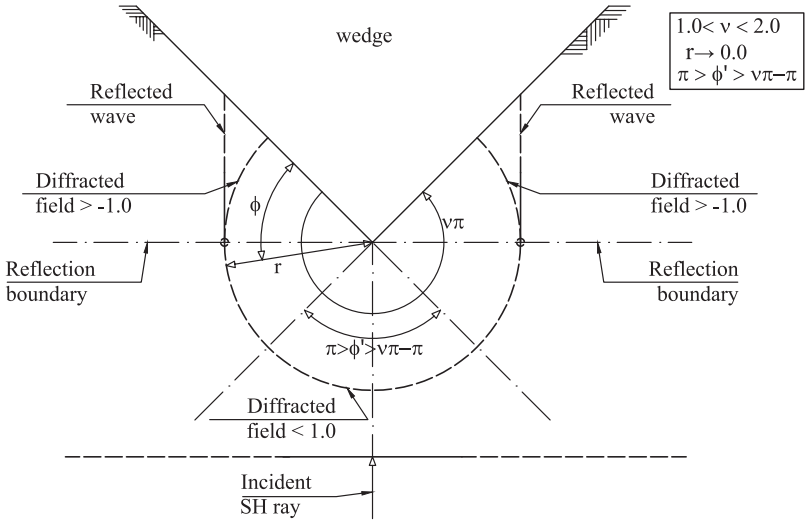

Figure 5. Solution at the wedge boundary under full illumination.

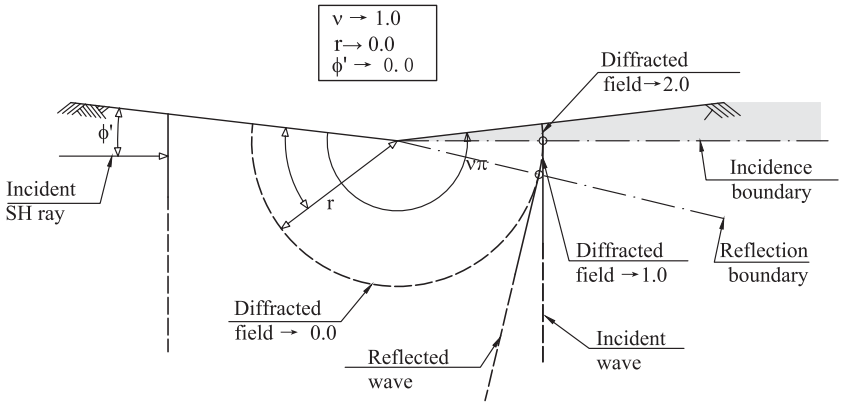

Figure 6. Particular case when the incident rays are parallel to the free boundary of the wedge.

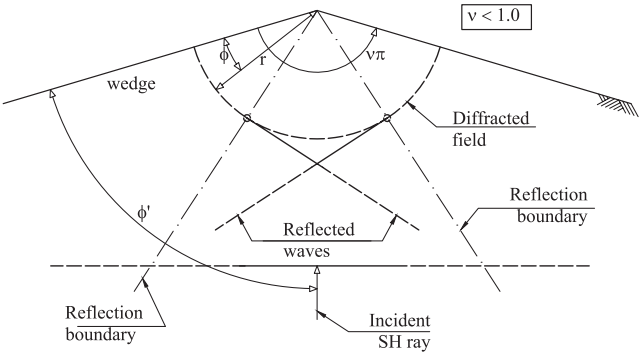

Figure 7. Particular case when $\nu < 1$ (i.e. propagation inside an infinite wedge).

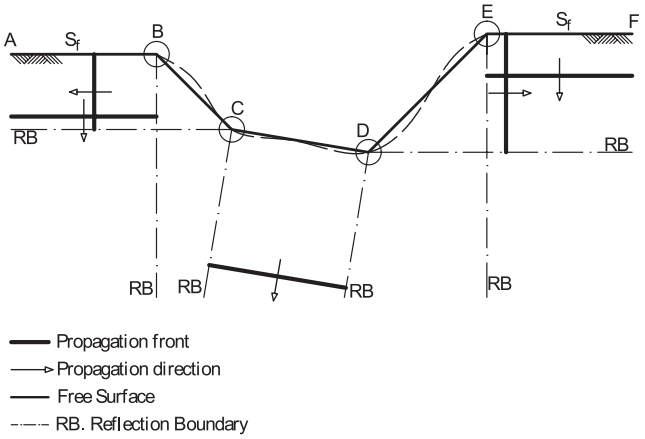

Figure 8. Schematic representation of a topographic irregularity at the free surface of a half-space. Reflection boundaries and diffraction sources are generated at each geometric singularity (i.e. corner point) where each one of the infinite wedges is truncated by a following continuing wedge.

the reflected field, corresponding to rays, that are reflected back and forth against the wedge boundaries. Depending on the number of reflections the amplitude may reach values which are several times the amplitude of the incident wave. In the particular case of a wedge with $\nu = 1/2$ it was shown by Sanchez-Sesma (1990) that at the apex the amplification with respect to the incident motion takes a value of 4.0. Moreover it was also shown that the amplification factor (AF) in the general case can be obtained with the simple expression $\mathrm{AF} = 2.0/\nu$.

5 A RECIPE TO BUILD THE SOLUTION TO THE SCATTERING PROBLEM

Consider the case of an arbitrary scatterer like the one represented by the dashed line in Fig. 8. Let us assume that the original shape is made up of surfaces with at least C^2-continuity, except at the transition points between the scatterer and the free surface of the half-space S_F (i.e. the points marked as B and E in the figure). If the incident front illuminates the whole surface, diffraction effects would take place only at the geometric singularities B, C, D and E. At those locations, the corresponding diffracted field could be exactly constructed using the solution for the generalized wedge from Kouyoumjian & Pathak (1974), that is, for a wedge with a flat and a curved boundary. The procedure to obtain the total solution reduces to the calculation of the incident, reflected and the diffracted fields. The contribution from the reflected field however, may be cumbersome to obtain since it corresponds to the case of a plane front incident against a smooth curved surface, and this implies computing the contribution from an infinite number of rays. Since the main interest here is to capture the diffraction effects, this complexity is avoided by considering domains conformed by flat segments only. In the generalized schematic problem, the arbitrary scatterer shown in thick dashed lines, is then represented by straight continuous segments defining the two semi-infinite boundaries A–B and E–F and the three finite boundaries, B–C, C–D and D–E, respectively. The resulting flat surfaces meet at corner geometric singularities, configuring wedges with diffraction sources. Each diffraction source gives rise to reflection boundaries (RB), dividing the domain into subdomains, with and without reflected fronts. Accordingly, with reference to Fig. 8, four diffraction sources corresponding to the encircled points B, C, D and E can be identified. The thick light grey lines show the reflected fronts propagating outwards. These rays are obtained using the slopes of the boundaries and the angle of the incident *SH* wave after using the classical reflection law. In the schematic problem, the semi-infinite surfaces A–B and E–F give rise to semi-infinite horizontal reflection fronts (propagating downwards) while the finite surfaces B–C, C–D and D–E, generate finite and perfectly bounded vertical reflection fronts (propagating outwards). The resulting subdomains enclosed by the reflection boundaries and without reflected fronts, correspond to the diffraction zones where continuity of the field must be restored. This is achieved with the fundamental wedge solution after adjusting the corresponding phase angle.

Each time the contribution from a diffraction source is generated, the resulting diffracted field would experience further

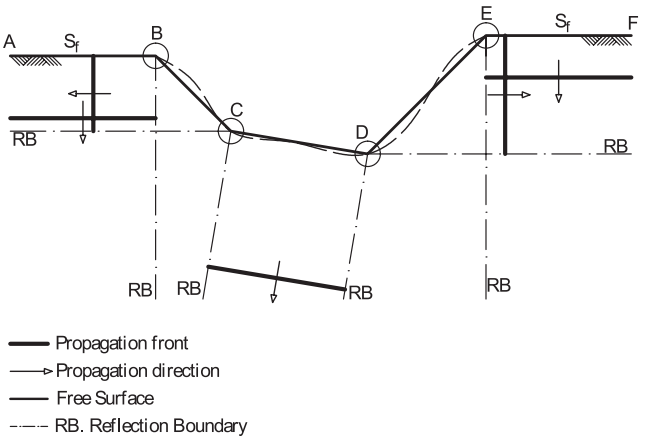

Figure 9. Canyon–hill combined surface topography in a half-space and definition of geometric parameters to be used in the application of (2).

(secondary) diffractions and reflections once it interacts with the adjacent wedges. This is a secondary diffraction effect, which can be obtained from the fundamental wedge solution in a recursive manner, after applying the case of a cylindrical incident front with a source at each wedge. The recursive algorithm is continued until the amplitude of the resulting diffracted field reaches values below a pre-selected threshold. Usually after considering a couple of iterations accounting for third-order diffraction effects, the amplitude is well below the one associated with the incident and reflected fields. The steps involved in the construction process are: (i) define the subdomain (or part of the domain) V^{in} illuminated by the incident field, (ii) define j subdomains V_j^R illuminated by k reflected fronts, (iii) identify subdomains V_i^0 of existence of an incoming field corresponding to the superposition of incident and reflected fronts and satisfying the condition $V^{\text{in}} \cap V_j^R = V_i^0$, (iv) consider the direct diffracted field resulting from the interaction of each plane front with associated geometric singularities and (v) consider the contribution from the secondary diffraction using a recursive application of the fundamental solution (2) for the case of incident cylindrical fronts.

6 APPLICATION TO THE SCATTERING BY A GEOMETRICAL PERTURBATION TO THE HALF-SPACE

The proposed analysis technique is now applied to the study of the particular surface topography described in Fig. 9. The relevant geometrical parameters are shown in the figure. For simplicity we submit the model to a vertically incident *SH* wave in the form of a Ricker pulse given by

$$R(t) = \left(2(\pi f_c \tau)^2 - 1\right) e^{\left(-(\pi f_c \tau)^2\right)},$$
$$\tau = t - 1 \text{ if } 0\,\text{s} \le t \le 4\,\text{s},$$
$$f_c = 2.0 \quad \text{Hz}, \tag{3}$$

where f_c = central frequency of the pulse and τ = time parameter used to define the start of the active phase. The medium is characterized by a shear wave propagation velocity $\beta = 1.0\,\text{km}\,\text{s}^{-1}$. The characteristic dimensions of the surface topography are $A2 = 1.0$ km, $A1 = 2.0$ km and $H = 1.0$ km with angles of 45°. The solution is first calculated in the frequency domain in the form of transfer functions relating the spectral displacement amplitude of the response to the one in the incident front. The final time domain response is obtained using the fast Fourier transform (FFT) algorithm.

The diffracted field w^{D} at a general point located inside the triangular subdomain enclosed by the reflection boundaries (shown in dashed lines) in Fig. 9 is given in (4)

$$\begin{aligned} w^{\text{D}} = {} & w^{\text{D}}(\theta_1, r_1)_{\text{C}} + w^{\text{D}}(\theta_2, r_2)_{\text{D}} + w^{\text{D}}(\theta_2, r_2, A2)_{\text{C-D}} + \\ & w^{\text{D}}(\theta_1, r_1, A2)_{\text{D-C}} + w^{\text{D}}(\theta_1, r_1, A2)_{\text{C-D-C}} \\ & + w^{\text{D}}(\theta_2, r_2, A2)_{\text{D-C-D}} + w^{\text{D}}\left(\theta_1, r_1, H\sqrt{2}\right)_{\text{B-C}} \\ & + w^{\text{D}}(\theta_2, r_2, A2)_{\text{B-C-D}} + w^{\text{D}}\left(\theta_2, r_2, 2H\sqrt{2}\right)_{\text{E-D}} \\ & + w^{\text{D}}(\theta_1, r_1, A2)_{\text{E-D-C}} + w^{\text{D}}\left(\theta_1, r_1, H\sqrt{2}\right)_{\text{C-B-C}} \\ & + w^{\text{D}}\left(\theta_2, r_2, 2H\sqrt{2}\right)_{\text{D-E-D}} + \ldots, \end{aligned} \tag{4}$$

where each term corresponds to an application of the fundamental solution by Kouyoumjian & Pathak (1974) given in (2). In this expression, each one of the double-argument terms accounts for the primary diffraction of the incident plane front. For instance a term like $w^D(\theta, r)_J$ refers to the diffraction of the incident plane front by the corner singularity J. Similarly a triple-argument term, refers to a higher order diffraction contribution. For instance the term $w^{\text{D}}(\theta, r_1, r_2)_{J-K}$ refers to the diffraction by the corner singularity K of the cylindrical front with source at J and resulting from the diffraction of the incident plane front at this last corner singularity. In this case the first argument r_1 refers to the distance between the field point and the secondary diffraction point (e.g. point K in the current case), while the second argument r_2 corresponds to the distance between the primary and secondary diffraction source (e.g. distance between J and K in the current case). Additional diffraction contributions could be considered until the amplitude is below some pre-defined threshold. On the other hand, the diffracted field generated by the different sources may experience additional reflections against the free surface. This contribution corresponds to the case of a cylindrical front incident against a free surface and its computation is straightforward. In this particular example we have not explicitly included those secondary reflections since its contribution is negligible as the numerical results will show.

To validate the accuracy of the constructed solution the problem was also solved using a direct boundary element method (BEM) algorithm. Figs 10 and 11 display snapshots of the propagation patterns at different instants during the propagation history, obtained with the superposition technique (left-hand column) and the BEM (right-hand column). In Fig. 10 the primary diffraction of the incident front generated by the corner singularities C and D appear as the light low-intensity cylindrical fronts joining the intense flat fronts generated upon reflection and corresponding to the terms $w^{\text{D}}(\theta_1, r_1)_{\text{C}}$ and $w^{\text{D}}(\theta_2, r_2)_{\text{D}}$ in (4). On the other hand, the bottom frame displays two diffracted sources: first the primary diffraction of the incident front at the corner singularity B and the secondary diffraction of the primary term $w^{\text{D}}(\theta_1, r_1)_{\text{C}}$ as it is diffracted at B. This corresponds to the term $w^{\text{D}}\left(\theta_1, r_1, H\sqrt{2}\right)_{\text{C-B-C}}$ in (4).

Fig. 11 shows the primary diffraction of the incident front by the uppermost corner singularity at E, once again appearing like a low-intensity cylindrical front. The remaining middle and bottom frames correspond to secondary diffraction sources described by terms like $w^{\text{D}}(\theta_2, r_2, A2)_{\text{B-C - D}}$ and $w^{\text{D}}(\theta_1, r_1, A2)_{\text{E-D - C}}$ in (4).

To evaluate the ability of the proposed technique in capturing the diffraction field, snapshots of the propagation patterns for this single displacement component were obtained using both, the analytical

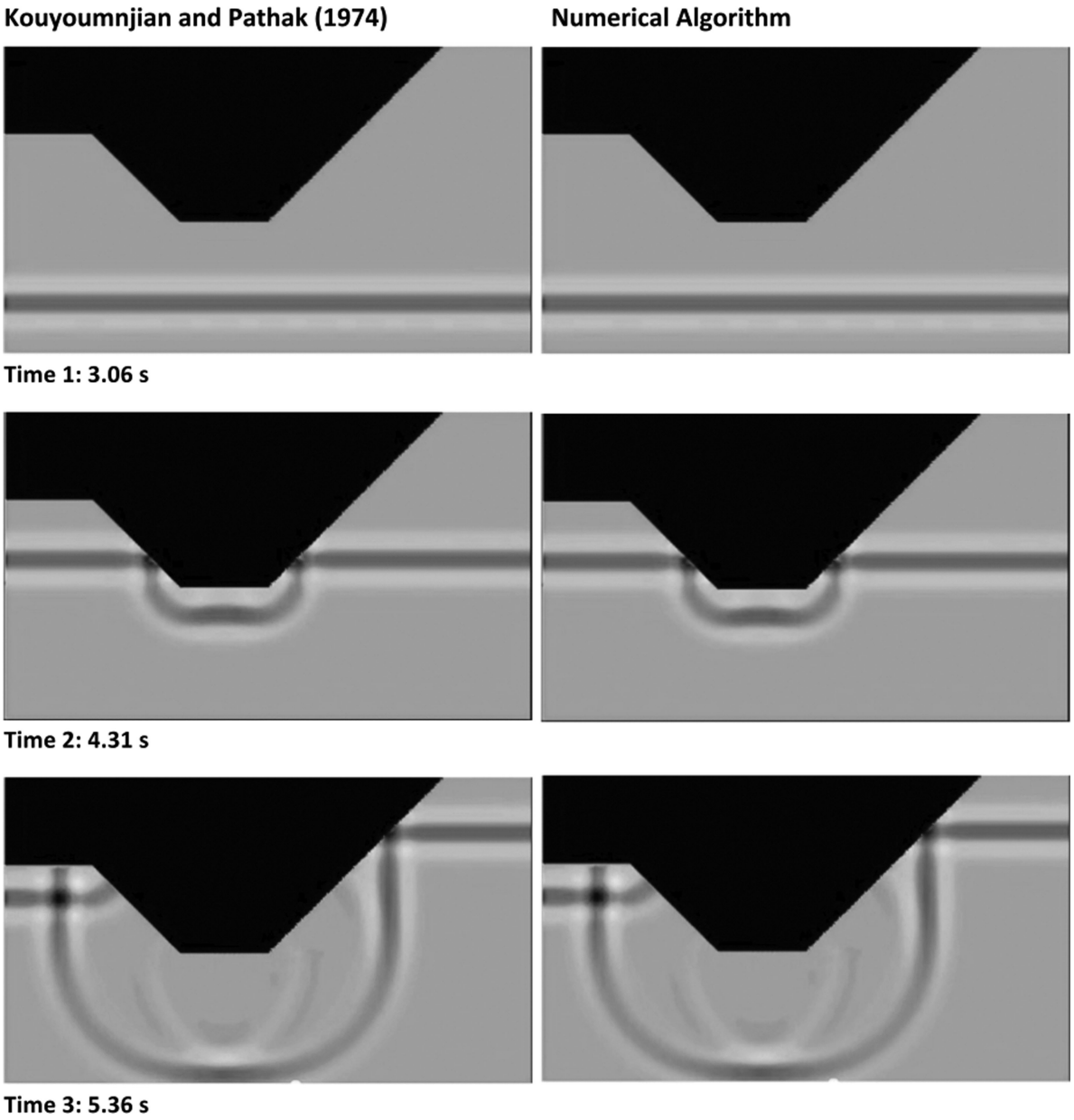

Figure 10. Snapshots of the propagation patterns for the surface topography shown in Fig. 8 obtained with the proposed technique (left-hand column) and the boundary element method algorithm (right-hand column). The top frame displays the unmodified incident front which is first diffracted by the singularities at C and D (middle frame) and then by the singularity at B.

approach and the numerical technique. The results are shown in Fig. 12. The maximum differences between both sets of results for this single displacement field correspond to 1.48 per cent and 3.57 per cent for the positive and negative values, respectively.

As a second validation, synthetic seismograms obtained with both methods at different observation points along the topographic irregularity were obtained. The corresponding results are displayed in Fig. 13. The response at the diffraction points 1, 3 and 5 is different from the one at points 2 and 6, where it is close to the one observed in a half-space with an amplitude of 2.0, but with some distortion due to the diffraction effects. At the observation points 1, 3 and 5 the arrivals of the incident, reflected and primary diffraction fields coincide. At point 3 a 1.0 s delayed arrival is observed. This corresponds exactly to the primary diffraction from the singularity at D. Later, exactly 2.4 s after the arrival of the incident wave, one observes the arrival of the primary diffraction from the corner singularity at B. Similarly, 5.6 s after the arrival of the incident front the arrival from the primary diffraction by the singularity at E is observed. At point 2, the strong phase at 1.2 s after the incident wave corresponds to the arrival from the primary diffraction generated at B. The same response is observed at point 6 at 2.4 s after the arrival from the incident front. The secondary diffractions are either too small or arrive in phase with some of the primary diffractions. For instance, the secondary diffraction at point 2, due to the neighbourhood wedges at B and C must arrive at 1.6 s and 2.6 s after the incident front, but these waves are not observed either with the BEM simulation or the analytic technique. To properly weight the effect of the diffraction field in the total solution, we compared the maximum and minimum values in the synthetic seismograms at the singularity point 5 in Fig. 9. Considering only up to third-order

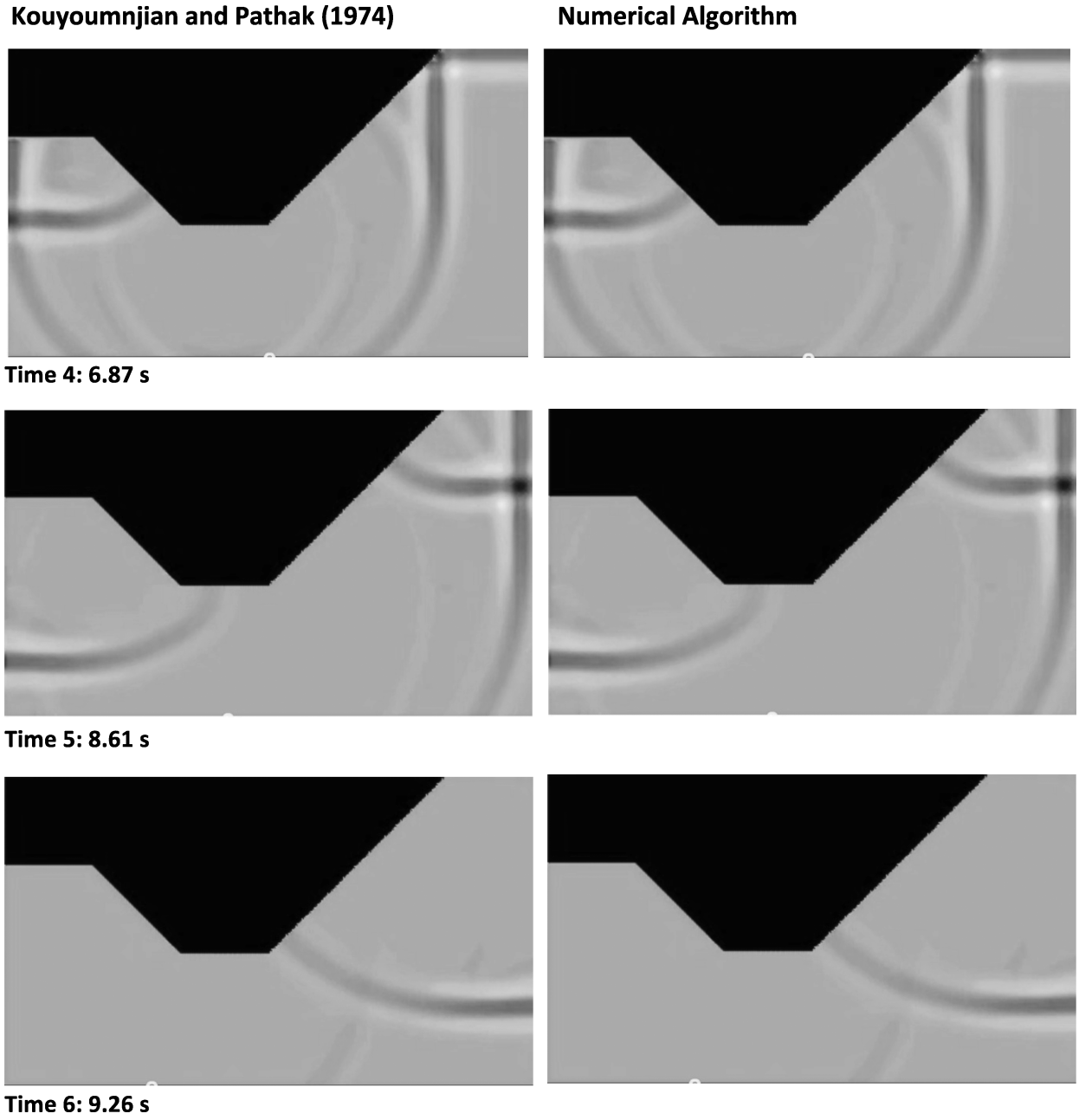

Figure 11. Snapshots of the propagation patterns for the surface topography shown in Fig. 8 obtained with the proposed technique (left-hand column) and the boundary element method algorithm (right-hand column). Only secondary diffraction effects remain as the primary fields have already travelled outside of the considered computational domain.

diffraction effects, that is a couple of iterations, we obtained the following values in the displacement amplitude: $A^{\max}_{\mathrm{BEM}} = 0.70769$, $A^{\max}_{\mathrm{APP}} = 0.6981$, $A^{\min}_{\mathrm{BEM}} = -1.5643$, $A^{\min}_{\mathrm{APP}} = -1.5118$ involving differences of 0.0096 in the former case and of 0.0525 in the latter, with an average difference in amplitudes of 0.0009. This average value is equivalent to 0.09 per cent of the incident field. These differences can be further reduced if fourth and higher order diffraction effects are considered.

7 CONCLUSIONS AND FURTHER WORK

We have presented a conceptual analysis tool based on superposition ideas, useful to study the scattering of *SH* waves by surface topographies of arbitrary shape resting in a half-space. The solution technique consists in the superposition of incident and reflected rays plus an additional contribution by a diffracted field. The diffracted field is obtained after adapting a solution identified in the context of diffraction of electromagnetic waves, and valid for a generalized wedge, to the scattering of mechanical *SH* waves. The method is approximated in the sense that it neglects surface-diffracted rays, while it retains corner-diffracted rays. To apply the superposition process, the arbitrary shape is represented by a finite series of continuous wedges. Over each one of the resulting wedges, the incident, reflected and generalized diffracted fields are obtained. Every time a wedge is rendered finite by its interception with a neighbourhood wedge, a reflection front appears. The analytical tool is described

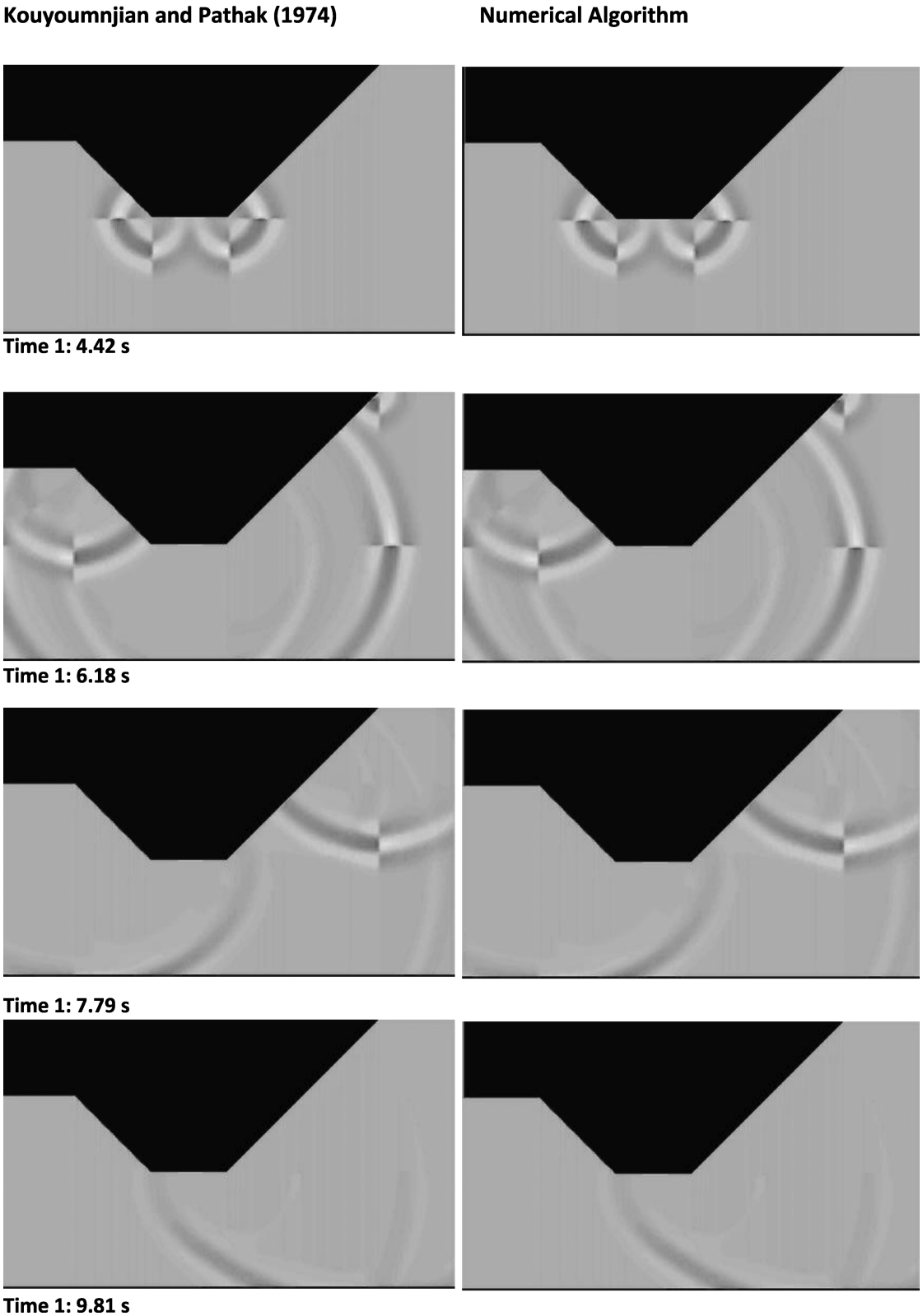

Figure 12. Snapshots of the propagation patterns corresponding to the diffracted field for the surface topography shown in Fig. 9 obtained with the proposed technique (left-hand column) and the boundary element method algorithm (right-hand column).

in terms of a recipe to undertake the superposition process. The solution can be made as accurate as needed since it can capture the diffraction of a diffracted field using the theory for an incident cylindrical wave.

The proposed construction method has been validated against results of numerical simulations using a BEM technique. The results obtained with the described methodology and in particular its comparison with the ones from the BEM technique presented in this

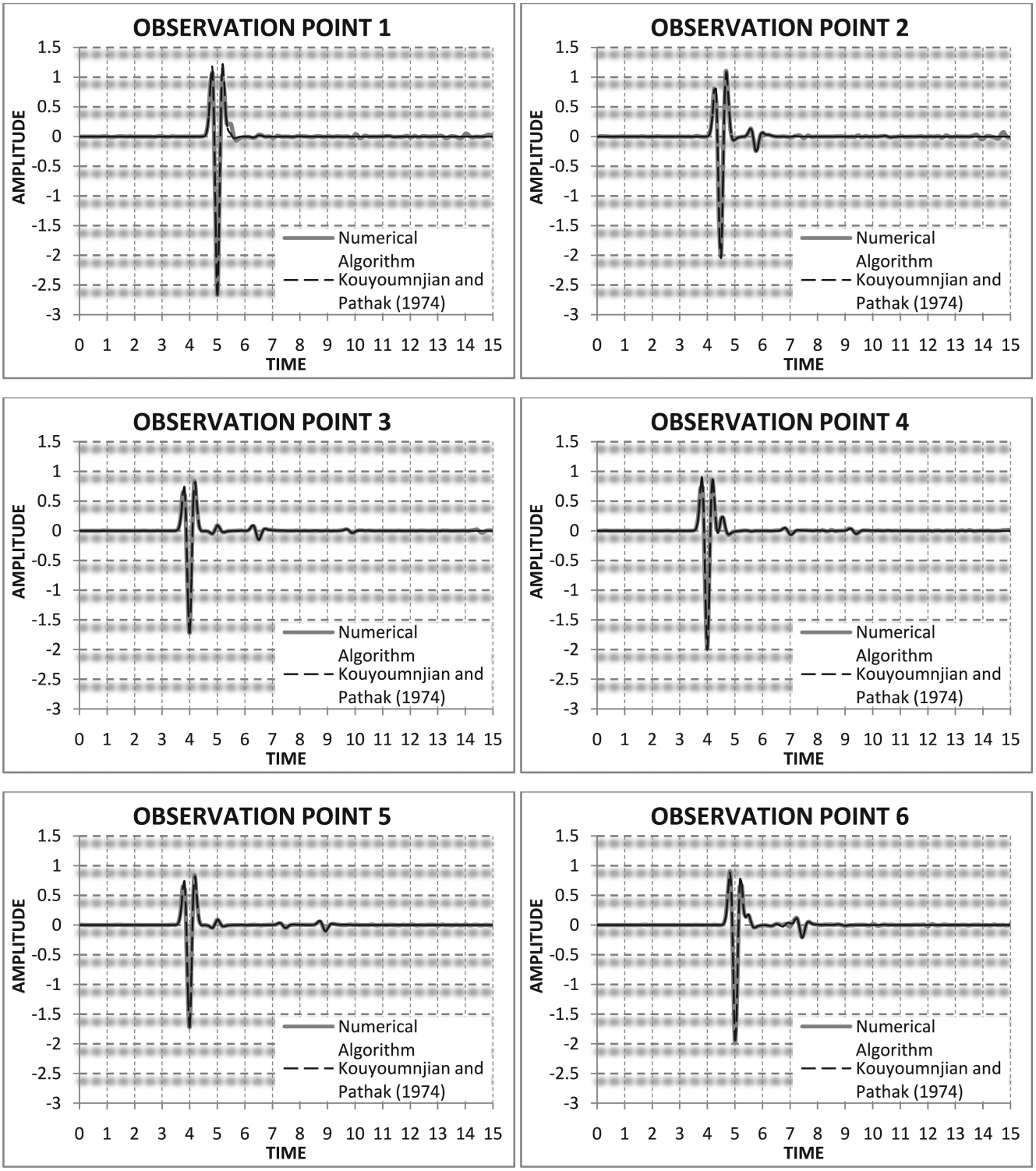

Figure 13. Time history of displacements at different observation points along the surface topography of Fig. 13 obtained with the analytic technique and the boundary element numerical scheme.

paper, suggest that these ideas can be extended to the case of more general problems. Moreover, the idea of separating the different contributions to the total field, can become a useful conceptual tool in the interpretation of numerical results in more realistic scenarios like the case of in-plane and 3-D motions and the case of a scatterer in the form of an elastic inclusion (or basin).

ACKNOWLEDGMENTS

This project was conducted with financial support from Departamento Administrativo de Ciencia, Tecnología e Innovación, COLCIENCIAS and from Universidad EAFIT through research grant number 1216-403-20661.

REFERENCES

Abo-Zena, A. & King, C., 1973. SH pulse in an elastic wedge, *Bull. seism. Soc. Am.,* **63**(5), 1571–1582.

Diankui, L. & Feng, H., 1991. Scattering of plane SH-waves by a cylindrica canyon of arbitrary shape, *Soil Dyn. Earthq. Eng.,* **10**(5), 249–255.

Forristal, G. & Ingram, J., 1971. Elastodynamics of a wedge, *Bull. seism. Soc. Am.,* **61**(2), 275–287.

Fu, L., 2005. Rough surface scattering: comparison of various approximation theories for 2D SH waves, *Bull. seism. Soc. Am.,* **95**(2), 643–663.

Hong, T. & Helmberger, D., 1977. Generalized ray theory for dipping structure, *Bull. seism. Soc. Am.,* **63**(5), 995–1008.

Hong, T. & Helmberger, D., 1978. Glorified optics and wave propagation in nonplanar structure, *Bull. seism. Soc. Am.,* **68**(5), 1313–1330.

Hudson, J., 1963. SH waves in a wedge-shaped medium, *Geophys. J. R. astr. Soc.,* **7**(5), 517–546.

Keller, J., 1962. Geometrical theory of diffraction, *J. Opt. Soc. Am.,* **52**(2), 116–130.

Klem-Musatov, K. & Aizenberg, A., 1984. The ray method and the theory of edge waves, *Geophys. J. R. astr. Soc.,* **79,** 35–50.

Kouyoumjian, R. & Pathak, P., 1974. A uniform geometrical theory of diffraction for an edge in a perfectly conducting surface, *Proc. IEEE,* **62**(11), 1448–1461.

Lee, V. & Luo, H., 2006. Antiplane (SH) waves diffraction by a semi-circular cylindrical hill revisited: an improved analytic wave series solution, *J. Eng. Mech. ASCE,* **132**(10), 1106–1114.

MacDonald, H., 1902. *Electric Waves,* Cambridge University Press, Cambridge, UK.

Sanchez-Sesma, F., 1985. Diffraction of elastic SH waves by wedges, *Bull. seism. Soc. Am.,* **75**(5), 1435–1446.

Sanchez-Sesma, F., 1990. Elementary solutions for response of a wedge-shaped medium to incident SH and SV waves, *Bull. seism. Soc. Am.,* **80**(3), 737–742.

Sanchez-Sesma, F. & Iturraran-Viveros, U., 2001. Scattering and diffraction of SH waves by a finite crack: an analytical solution, *Geophys. J. Int.,* **145,** 749–758.

Sanchez-Sesma, F. & Velasquez, S., 1987. On the seismic response of a dipping layer, *Wave Motion,* **9**(5), 387–391.

Sanchez-Sesma, F., Chavez-Garcia, F. & Bravo, M., 1988. Seismic response of a class of alluvial valleys for incident SH waves, *Bull. seism. Soc. Am.,* **78,** 83–95.

Sommerfeld, A., 1896. Mathematische theorie der diffraktion, *Math. Ann,* **47,** 317–374.

Todorovska, M. & Lee, W., 1990. A note on the response of a shallow circular valleys to Rayleigh waves: analytical approach, *Earthq. Eng. Vibrat.,* **10,** 21–34.

Todorovska, M. & Lee, V., 1991a. Surface motion of circular alluvial valleys of variable depth for incident plane sh waves, *Soil Dyn. Earthq. Eng.,* **10,** 192–200.

Todorovska, M. & Lee, V., 1991b. A note on scattering of Rayleigh waves by shallow circular canyons: analytical approach, *Bull. Ind. Soc. Erarthq. Technol.,* **28**(306), 1–16.

Trifunac, M., 1971. Surface motion of a semi-cylindrical alluvial valley for incident plane SH waves, *Bull. seism. Soc. Am.,* **61**(6), 1755–1770.

Trifunac, M., 1973. Scattering of plane SH waves by a semi-cylindrical canyon, *Earthq. Eng. Struct. Dyn.,* **1,** 262–281.

Tsaur, D., 2010. Exact scattering and diffraction of antiplane shear waves by a vertical edge crack, *Geophys. J. Int.,* **181,** 1655–1664.

Tsaur, D., 2011. Scattering and focusing of SH waves by a lower semielliptic convex topography, *Bull. seism. Soc. Am.,* **101**(5), 2212–2219.

Tsaur, D., Chang, K. & Hsu, M., 2010. An analytical approach for the scattering of SH waves by a symmetrical v-shaped canyon: deep case, *Geophys. J. Int.,* **183,** 1501–1511.